Communications Research Centre

A THEORY OF 'SQUINTED' SYNTHETIC-APERTURE RADAR

by

M.R. Vant and G.E. Haslam

DEPARTMENT OF COMMUNICATIONS
MINISTÈRE DES COMMUNICATIONS

CRC REPORT NO. 1339

CANADA

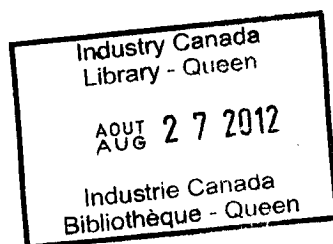OTTAWA, NOVEMBER 1980
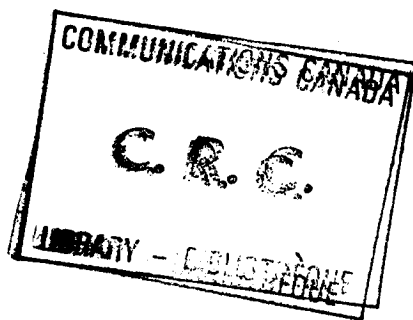
COMMUNICATIONS RESEARCH CENTRE

DEPARTMENT OF COMMUNICATIONS
CANADA

A THEORY OF 'SQUINTED' SYNTHETIC-APERTURE RADAR

by

M.R. Vant and G.E. Haslam

(Radar and Communications Technology Branch)

CRC REPORT NO. 1339

November 1980

OTTAWA

TABLE OF CONTENTS

A THEORY OF 'SQUINTED' SYNTHETIC-APERTURE RADAR

by

M.R. Vant and G.E. Haslam

ABSTRACT

A theory is developed that describes the processing
of data collected with a satellite-borne or airborne
synthetic-aperture radar (SAR). A description of the
target-radar geometry, and the form of the received,
demodulated radar signal is given. It is shown that
the solution for the case in which the antenna is
directed perpendicular to track (sidelooking), is
obtained by a simplification of the general case in
which the antenna is squinted with respect to the
perpendicular to track.

A mathematical description of the signal proces-
sing operations required to produce a SAR image from
the received radar signal is presented and the form
of the processed signal is described. In particular,
a technique which employs two-dimensional matched
filtering to produce the radar image is discussed and
the ability of this approach to accommodate the
coupling of the range (across-track) and azimuth
(along-track) signals is investigated. In addition,
the extensions to the theory required for non-coherent
averaging are included.

1. INTRODUCTION

In this report a description of the mathematical operations required
to produce geometrically correct images from airborne or satellite-borne
synthetic-aperture radars (SARs) by means of convolution with the impulse
response of a two-dimensional matched filter, is given. In contrast to
other theories [1-14], this report describes a two-dimensional technique

that applies to data acquired in either a 'squinted' or 'sidelooking'
configuration. In the 'sidelooking' configuration the radar antenna is
pointed so that the direction of the centre of the beam is perpendicular to
ground track [3]. In the 'squinted' configuration the antenna points in a
direction other than the perpendicular [14].

In order to convert the raw radar data to an image, it is generally
required that a two-dimensional signal processing operation be performed.
Conventionally, this operation is segmented into two, one-dimensional
operations where the radar return signals that are associated with the range
(across-track) and azimuth (along-track) coordinates are independently cross-
correlated with their respective reference functions. Provided the range
and azimuth signals are orthogonal, and provided the azimuth signal extent
is small, this approach works well.

The signal processing is more complicated if the SAR antenna is
'squinted', or if the azimuth extent of the signal is large. In these
instances the range and azimuth signals are coupled, i.e., they are not
independent of each other, and the operations required to produce a high
quality distortion-free image are more complicated.

In the following sections the form of the coupled signal is examined,
and the mathematical operations required to produce a high quality image are
described. In particular a novel technique that employs two-dimensional
cross-correlation of the received SAR signal with a two-dimensional reference
function is described. An approximate closed formed solution is given for
the two-dimensional correlation integral and its form is examined. It is
shown that a single cross-correlation function can be used to produce high
quality images from radar signals obtained over a swath in range, but that
these images must be geometrically corrected to remove positional errors
introduced by the processing. Equations are derived to describe the positional
errors and the operations required to remove them. Finally, the modifications
required to extend the theory to 'multilook' processing, or noncoherent
averaging, are developed.

2. RANGE AS A FUNCTION OF AZIMUTH POSITION

In order to characterize the SAR signal that results when the trans-
mitted signal, reflected from a point target that is fixed to the planet,
is returned to the radar, it is necessary to describe the range to the
target as a function of the radar's position in its orbit. To do this, the
flight direction of the radar relative to the surface of the planet is
derived. From this result, an equation describing the range to the point
target as a function of the satellite's orbital position is obtained. The
satellite's orbital position is measured relative to the position in the
orbit at which the point target is in the centre of the antenna's horizontal
pattern.

The velocities of the vehicle and the planet are calculated in the
following manner: The planet is assumed to be a sphere of radius r_e rotating
with angular velocity ω_e, and the satellite is assumed to be travelling along
a circular orbit at angular velocity ω_s (see Figure 1). The tangential

velocity $\underline{V}_s$, of the radar, with respect to the inertial frame is $\omega_s(r_e+h_s)$, where h_s is the altitude of the satellite above the surface of the planet. The subsatellite point S_1 (see Figure 2), is the point of intersection of the surface of the planet and the line joining the radar and the centre of the planet (see Figure 3). The point S_1 has a tangential velocity $\underline{V}_s/C_a$, with respect to the inertial frame, where the constant C_a is defined as

$$C_a = 1 + \frac{h_s}{r_e} .$$

(1)

The surface of the planet is moving beneath S_1 at a tangential velocity $\underline{V}_e$, defined with respect to the inertial frame

Figure 1. Angles that define orbit. $V_{\underline{s}}/c_a$ and $V_{\underline{eq}}$ are tangential to the planet surface.

Figure 2. Vehicle Equivalent Velocity

SPACECRAFT

Figure 3. Radar Geometry

The point S_1 has a velocity V_{eq} with respect to the rotating surface. The magnitude of V_{eq} is

$$|V_{\underline{eq}}| = \left[V_{en}^2 + \left(\frac{V_s}{C_a} - V_{ep} \right)^2 \right]^{\frac{1}{2}} . \tag{2}$$

and its direction relative to V_s/C_a is (see Figure 2)

$$\theta_{ye} = \tan^{-1} \left| \frac{V_{en}}{\frac{V_s}{C_a} - V_{ep}} \right| . \tag{3}$$

The velocities V_{en} and V_{ep} are the components of V_e normal to, and parallel to $V_{\underline{s}}/C_a$, respectively. In Appendix A, V_{en} and $\overline{V_{ep}}$ are shown to be

$$V_{ep} = \omega_e r_e \cos\theta_i , \tag{4}$$

and

$$V_{en} = \omega_e r_e \sin\theta_i \cos\phi_o , \tag{5}$$

where θ_i is the angle of inclination of the orbit, and ϕ_o is the position of the spacecraft in the orbital plane measured from the equator (see Figure 1).

Equations (2) and (3) are valid for the vehicle in an ascending or descending orbit.

It is assumed that the radar antenna is pointed at an angle α with respect to ground track as shown in Figure 3. In this report the angle θ_y will be called the squint angle. The angle

$$\alpha = \frac{\pi}{2} - \theta_y, \tag{6}$$

is then the complement of the squint angle. This angle is composed of two components, i.e.,

$$\theta_y = \theta_{ye} + \theta_{ya} \tag{7}$$

where θ_{ye} is caused by planet rotation and θ_{ya} is the antenna pointing angle relative to the perpendicular to $\underline{V}_s$. The angles θ_{ye} and α are defined with respect to the equivalent velocity vector $\underline{V}_{eq}$, as shown in Figure 2, for the case $\theta_{ya}=0$.

The slant range from the radar located at S_2', to a point target A on the planet's surface (see Figure 3), is

$$r_2 = [r_e^2 + (r_e+h_s)^2 - 2r_e(r_e+h_s)\cos\theta_2]^{\frac{1}{2}}, \tag{8}$$

where θ_2 is the angle subtended by the arc AS_2 on the surface of the planet when S_2 is the sub-satellite point.

Equation (8) can be rewritten to show how r_2 varies with both the satellite's orbital position and the complementary squint angle α. From spherical trigonometry and Figure 3 it can be shown that

$$\cos\theta_2 = \cos\theta_r \cos(\theta_a+\theta_b), \tag{9}$$

and

$$\sin\theta_a = \frac{\cos\alpha\sin\theta}{\cos\theta_r} . \tag{10}$$

The angles θ_r, θ_a, θ_b and θ are defined as follows: θ_r is the angle subtended at the planet's centre by the arc AS_0, where S_0 is the sub-satellite point when the satellite is located at its point of closest approach to A; θ_a is the angle which defines the satellite's position in the orbit where the radar antenna is pointing directly at the target at A; θ_b is the angle measured relative to θ_a which defines the present position of the satellite; and θ is the angle subtended by the arc AS_1 on the surface of the planet, when S_1 is the sub-satellite point. If one expands $\cos(\theta_a+\theta_b)$ in (9) and substitutes for $\sin\theta_a$, by using (10), the equation for r_2 can be rewritten as a function of θ_b.

$$r_2(\theta_b) = \left\{r_e^2 + (r_e+h_s)^2 - 2r_e(r_e+h_s) \left[\cos\theta\cos\theta_b - \sin\theta\cos\alpha\sin\theta_b\right]\right\}^{\frac{1}{2}}. \tag{11}$$

It is more convenient to work with $r_2(\theta_b)$ expressed as a polynomial, than with the form given by (11). The polynomial form is obtained by expanding $r_2(\theta_b)$ in a Mclaurin series about θ_a. Previous treatments [1] have expanded $r_2(\theta_b)$ about $\theta_a=0$. An expansion about $\theta_a=0$ is adequate when there is no squint, i.e., $\alpha = \pi/2$ rad; however for a $\alpha \neq \pi/2$ rad. an expansion about θ_a as given by (10), yields a series which requires fewer terms to represent $r_2(\theta_b)$ accurately.

A Mclaurin series expansion for $r_2(\theta_b)$, about angle θ_a is

$$r_2(\theta_b) = \sum_{p=0}^{\infty} \frac{r_2^{(p)}(0)}{p!} \theta_b^p. \tag{12}$$

The first three derivatives of the series evaluated at $\theta_b=0$ are:

$$r_2(0) = r_1 \tag{13}$$

$$r_2^{(1)}(0) = \frac{r_e(r_e+h_s)}{r_1} \frac{\sin\theta_r}{\tan\alpha} \tag{14}$$

$$r_2^{(2)}(0) = \frac{r_e^2 + (r_e+h_s)^2}{2r_1} - \frac{r_1}{2} - \frac{[r_2^{(1)}(0)]^2}{r_1} \tag{15}$$

and

$$r_2^{(3)}(0) = -r_2^{(1)}(0)\left[-\frac{1}{2} + \frac{3}{2}\frac{r_e^2 + (r_e+h_s)^2}{r_1^2} - \frac{3[r_2^{(1)}(0)]^2}{r_1^2}\right] \tag{16}$$

where r_1 is the slant range to point A at angle θ_a. It can be shown that in most cases the terms in θ_b^3 and above in (12) can be neglected. Thus $r_2(\theta_b)$ can be written

$$r_2(s) = a_0 + a_1s + a_2s^2, \tag{17}$$

where s is the arc length along the ground track and is given by

$$s = \theta_b r_e, \tag{18}$$

and,

$$a_0 = r_1, \tag{19}$$

and,

$$a_1 = \frac{r_e}{r_1} C_a \frac{\sin\theta_r}{\tan\alpha}, \tag{20}$$

and,

$$a_2 = \frac{1}{2}\left[\frac{1}{2r_1}(1+C_a^2) - \frac{r_1}{2r_e^2} - \frac{a_1^2}{r_1}\right]. \tag{21}$$

Equation (17) is the general expression for the slant range to a point reflector.

For $\alpha=\pi/2$ (17) simplifies to

$$r_2(s) = a_0 + a_2 s^2 \tag{22}$$

where

$$a_0 = r_o \tag{23}$$

$$a_1 = 0 \tag{24}$$

$$a_2 = \frac{1}{2}\left[\frac{1}{2r_o}(1+C_a^2) - \frac{r_o}{2r_e^2}\right], \tag{25}$$

and r_o is the slant range to point A when the radar is at its point of closest approach to A.

A general expression for range as a function of time (or orbital position θ_b), is given by (17). Equation (17) is an approximation that is valid for a small angular extent about θ_a. The error introduced by approximating (11) by (17) can be evaluated by calculating the difference between these two equations for the θ_b values of interest.

In the derivation of (17) a circular orbit and a spherical planet, i.e., constant h_s were assumed. This constraint can be relaxed so that an elliptical orbit and ellipsoidal planet can be accommodated. Appendix B gives the derivation of an extended version of (11) which includes a constant vertical velocity V_v. Obviously, for the more general case of an elliptical orbit, neither V_{eq} nor V_v is truly constant. However for realistic orbits, accelerations $\dot{V}_{eq}$ and $\dot{V}_v$ are small.

3. THE FORM OF THE TWO-DIMENSIONAL SIGNAL FOR A POINT TARGET

In this treatment of SAR it is assumed that the surface causing the radar backscatter can be modelled by a collection of point scatterers. The SAR illuminates and receives the signal scattered from these scatterers. In this section this signal is described. Subsequent sections will discuss the signal processing that operates upon the received signal from each point scatterer and produces an image of each point.

The term two-dimensional is used to describe the signal because the received signal is formed by gathering information from each pulse transmitted (the range dimension), and from changes that occur in the received

signal from pulse to pulse (the along track or azimuth dimension), as a result of the relative motion between the radar and the scatterer. The derivation of the form of the two-dimensional signal consists of the following steps:

1. the determination of the form of the transmitted signal;

2. the derivation of the form of the signal received by the radar when this transmitted signal is reflected back to the radar by a point target; and

3. the derivation of the form of the signal obtained by mixing in a quadrature detector, the received signal with the carrier of the transmitted signal.

It will be described in later sections how this two-dimensional signal is processed to form the two-dimensional radar image of the point target.

3.1 FORM OF THE TRANSMITTED SIGNAL

As the vehicle upon which the radar is mounted proceeds along its flight path, the radar transmits a series of pulses (see Figure 4) of the form

$$f_T(t) = \left\{ R_e \sum_{m=-\infty}^{\infty} W(t)\psi(t-mT)\exp[j(\omega_c t+\phi_o)] \right\} , \tag{26}$$

where $\psi(t-mT)$ is a complex modulation function, $W(t)$ is a weighting function which will be defined later, t is time, T is the interpulse period, m is the pulse number, ϕ_o is the phase of the carrier at $t=0$, and ω_c is the carrier frequency. The argument $(t-mT)$ of the modulation function represents time measured from the start of the mth pulse. It is assumed for convenience that $m=0$ when the satellite is located at S_1' (see Figure 3), i.e., at an angle θ_a from the position occupied by the satellite when it is at the point of closest approach S_o'.
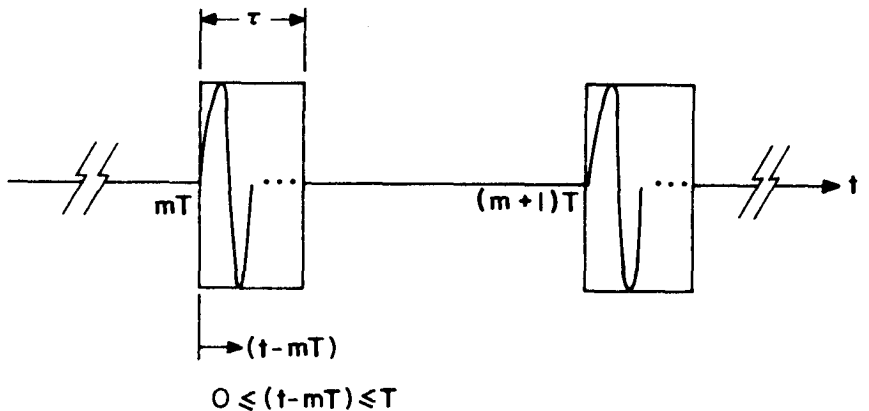

Figure 4. Transmitted Signal

3.2 FORM OF THE RECEIVED SIGNAL

The signal transmitted at time t from position S_T' (Figure 11), and received at time $t+\Delta t$ at position S_R', after reflection from the point target at A, is given by

$$f_R(t) = \text{Re}\left\{\Gamma W^2(t)\psi(t-mT-\Delta t)\right.$$

$$\left.\exp\left\{j[\omega_c(t-\Delta t) + \phi_o]\right\}\right\} \qquad (27)$$

where, Δt is the time taken by the signal to travel the path $S_T'AS_R'$ (Figure 11), and Γ is the reflection coefficient of the point scatterer at A. It is assumed that the point target at A is aspect insensitive so that Γ does not change during the time the radar views the target.

The range to the target changes during the time taken to travel the path $S_T'AS_R'$ (Figure 11). It is shown in Appendix C that a very good approximation for Δt is

$$\Delta t \simeq \frac{2r_2(s)}{c} \quad . \qquad (28)$$

3.3 FORM OF THE SIGNAL OUTPUT BY THE QUADRATURE DETECTOR

The received signal $f_R(t)$ is demodulated in a quadrature detector by mixing $f_R(t)$ with the carrier of $f_T(t+\Delta t)$. The transit time Δt can be replaced by $2(a_0+a_1s+a_2s^2)/c$ using (17) and (28), and then the complex signal output by the quadrature detector can be expressed as the two-dimensional function

$$f_D(t',s) = \frac{\Gamma}{2} W^2(t',s)\psi\left[t' - \frac{2}{c}(a_0+a_1s+a_2s^2)\right] \exp[-j2k(a_0+a_1s+a_2s^2)], \qquad (29)$$

where,

$$t' = t-mT, \qquad (30)$$

is time measured from the start of the mth pulse,

$$s = mV_{eq}T, \qquad (31)$$

is the arc length travelled by the sub-satellite point along the sub-satellite track during m interpulse periods, and

$$k = \frac{\omega_c}{c} \quad , \qquad (32)$$

is the wave number. The variable t' is a measure of slant range. The specific value of t' given by Δt (28) refers to the transmit time for a target at a specific slant range r_2.

In eqn. (29) $W^2(t)$ has been rewritten as the two-dimensional function $W(t',s)$ by segmenting $W(t)$ into consecutive sections, of length T, and using the variable 's' to index the sections.

The weighting function $W^2(t',s)$ does two things: it limits the range extent of the strip of terrain from which signals are received; and it limits the number of pulses which can be coherently integrated to form the SAR image of the target at A. In limiting the number of pulses that can be coherently integrated, $W^2(t',s)$ also limits the maximum azimuth resolution attainable.

It is assumed that the position and width of $W^2(t',s)$ in the t' dimension are chosen so that the radar illuminates only a narrow strip of the planet's surface, containing targets at slant ranges in the interval

$$\frac{c}{2} nT \leq r_2 \leq \frac{c}{2} (n+1)T, \tag{33}$$

where n is an integer. There is a range ambiguity, therefore the value of n must be known to convert Δt correctly into r_2 via (28).

When $W^2(t',s)$ is chosen to satisfy (33), signals at ranges

$$r_2' = r_2 \pm p \frac{c}{2} T, \qquad p = 1,2,\ldots, \tag{34}$$

which would otherwise arrive at the radar during the time interval $[nT \leq t' \leq (n+1)T]$ and produce ambiguous signals superimposed on the desired signal, do not have to be considered. It is also assumed that the interval of r_2 which satisfies (33) is large compared to the range extent in t' of the modulation function ψ in (29), and that $W^2(t',s)$ varies slowly with t'. With these assumptions $W^2(t',s)$ can be written as

$$W^2(t',s) = W_0 W_1(s) , \tag{35}$$

where W_0 is a constant.

The shape of $W_1(s)$ in the s-dimension is assumed for ease of analysis to be rectangular. The actual shape of $W_1(s)$ is determined by the antenna pattern. The following analysis will differ in the details but not the general concept if a different $W_1(s)$ is used. Equation (34) for $W^2(t',s)$, can be written

$$W^2(t',s) = W_0 \operatorname{rect}\left(\frac{s}{L_S}\right) , \tag{36}$$

where L_S is the synthetic-aperture length. The size of L_S determines the number of pulses, returned from the point target at A, which can be coherently processed to form the SAR image of A.

The general two-dimensional signal for a unity gain point target is obtained by setting Γ to unity in (29), i.e.,

$$h_1(t',s) = W_0 \operatorname{rect}\left(\frac{s}{L_S}\right)\psi\left[t' - \frac{2}{c} (a_0+a_1s+a_2s^2)\right] \exp[-j2k(a_0+a_1s+a_2s^2)]. \tag{37}$$

Figure 5 shows the form of $h_1(t',s)$. The responses from three point targets are shown. At some particular instant in time targets (1) and (2) both lie in the same direction α but are at different r_1's. Target (3) lies at the same range r_0, as target (1), but is situated at a different α.

The thick solid lines in Figure 5 represent the envelope of $h_1(t',s)$. The lines limiting the s extent are the edges of the $rect(s/L_S)$ function. This function increases in length as the radar's antenna pattern broadens with range. In other words the arc length L_S over which the radar views the target increases with range.

The curved lines limiting the t' extent of the signal are the edges of $|\psi|$ in (37). The curvature of these lines is determined by the manner in which r_2 varies with s (shown by the dashed lines in Figure 5).

The thin solid lines inside the ψ-envelope represent constant phase contours of ψ. The phase of ψ is composed of two factors: the phase $\exp[-j2k(a_0+a_1s+a_2s^2)]$ along the 's' coordinate (see Figure 5), and the phase of ψ along the t' coordinate.

4. SIGNAL COMPRESSION

The signal (29) returned from the point target at A (Figure 3) must be processed to produce a two-dimensional image of the target. The goal of this section is to show the form of the solution resulting from the two-dimensional convolution of the signal received from a point target ($\Gamma=1$) with the two-dimensional impulse response of a filter that is matched to the signal at a particular reference range. A mathematical analysis, that results in an approximate closed-form solution for the equation describing the image, is presented.
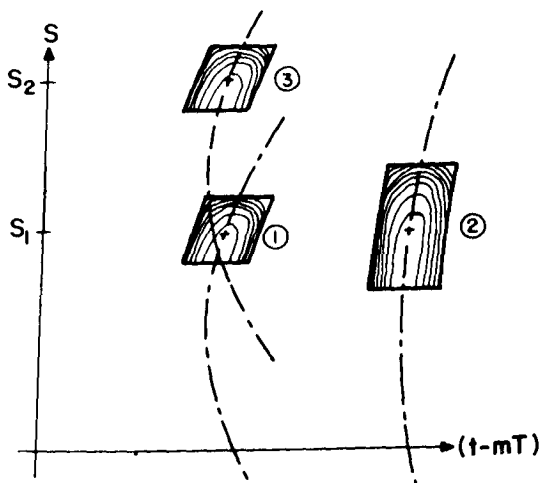

Figure 5. The form of the signals received from three point targets. Targets (1) and (2) are illuminated by the antenna at the same time. Target (3) is at the same r_o as target (1) but is illuminated at a later time.

In performing the analysis the general point target is assumed to be at range r_1 and complementary squint angle α, and to have an associated synthetic-aperture length L_S. the two-dimensional impulse response of the matched filter is calculated for a point target with a reflection coefficient of unity, located at a reference range $\tilde{r}_1$, and complementary squint angle $\tilde{\alpha}$, and which has a synthetic aperture length $\tilde{L}_S$. The values r_1, α and L_S are chosen to be different from the reference values $\tilde{r}_1$, $\tilde{\alpha}$ and $\tilde{L}_S$. This is done so that the effect of mismatch between the signal and reference function can be examined in the final closed form solution for the SAR image.

4.1 THE TWO-DIMENSIONAL MATCHED FILTER

The impulse response of the matched filter is the time-reversed conjugate of the two-dimensional signal returned from a point target (37). When the parameters used in (37) are changed to the reference values, the impulse response of the matched filter can be written as

$$h_2(t',s) = \tilde{h}_1^*(-t',-s) \tag{38}$$

i.e.,

$$h_2(t',s) = \text{rect}\left(\frac{-s}{\tilde{L}_S}\right)\psi*\left[-t' - \frac{2}{c}(\tilde{a}_0-\tilde{a}_1 s+\tilde{a}_2 s^2)\right] \exp[j2k(\tilde{a}_0-\tilde{a}_1 s+\tilde{a}_2 s^2)], \tag{39}$$

where the $\tilde{a}_0$, $\tilde{a}_1$, and $\tilde{a}_2$ refer to the reference values of a_0, a_1, and a_2, which are found by substituting $\tilde{r}_1$ and $\tilde{\alpha}$ in (19)-(21).

In the actual analysis a slightly modified form of (39), in which the $\tilde{a}_0$ term has been removed, will be used

$$h_3(t',s) = \text{rect}\left(\frac{-s}{\tilde{L}_S}\right)\psi*\left[-t' - \frac{2}{c}(-\tilde{a}_1 s+\tilde{a}_2 s^2)\right] \exp[j2k(-\tilde{a}_1 s+\tilde{a}_2 s^2)]. \tag{40}$$

The use of $h_3(t',s)$ instead of $h_2(t',s)$ causes targets to be mapped at range a_0 instead of range $a_0-\tilde{a}_0$ in the final SAR image. In other words a shift of the map origin is introduced.

4.2 SOLUTION OF THE TWO-DIMENSIONAL CONVOLUTION INTEGRAL

An equation describing the form of the output SAR image is obtained by solving the two-dimensional convolution integral

$$f_0(t',s) = \iint\limits_{-\infty}^{\infty} h_3(t'-\Omega,s-\xi)f_D(\Omega,\xi)d\Omega d\xi = \frac{W_o \Gamma}{2} \int\limits_{-\infty}^{\infty} \text{rect}\left(\frac{-s+\xi}{\tilde{L}_S}\right)\text{rect}\left(\frac{\xi}{L_S}\right)$$

$$\exp\left\{-j2k[a_0+a_1\xi-\tilde{a}_1(\xi-s) + a_2\xi^2-\tilde{a}_2(\xi-s)^2]\right\}$$

$$\int\limits_{\Omega=-\infty}^{\Omega=\infty} \psi*\left\{-t'+\Omega - \frac{2}{c}[\tilde{a}_1(\xi-s) + \tilde{a}_2(\xi-s)^2]\right\} \psi\left[\Omega - \frac{2}{c}(a_0+a_1\xi+a_2\xi^2)\right] d\Omega d\xi. \tag{41}$$

The solution to (41) will be obtained in three steps. The first step will be to solve the inside integral by integrating over Ω. The second step will be to place a restriction on the ξ variation of the solution to the inside integral. Provided certain conditions are satisfied this restriction will allow a separation of the variables. The third step will be to solve the outside integral which is a function of ξ.

4.2.1 Solution of the Inside Integral

The solution to the inside integral is $g(\gamma)$ where

$$\gamma = t' - \frac{2}{c} [a_0+a_1\xi-\breve{a}_1(\xi-s)+a_2\xi^2-\breve{a}_2(\xi-s)^2] \tag{42}$$

The function $g(\gamma)$ is the auto-correlation of ψ, and has its maximum at

$$t' = \frac{2}{c} [a_0+a_1\xi-\breve{a}_1(\xi-s)+a_2\xi^2-\breve{a}_2(\xi-s)^2]. \tag{43}$$

The form of the modulation function ψ has not yet been specified. Modulation functions used for pulse-compression normally have the characteristic that most of the energy in the output pulse is confined to a main peak which has a 3 dB width approximately equal to $\pi c/K\tau$, where $2\pi/K\tau$ is the bandwidth in Hz. In this report only modulation functions of this type will be considered.

The shape of the $g(\gamma)$ function that is obtained for a typical modulation code $\psi(t')$ is examined next. If a linear FM modulation function is assumed, $\psi(t')$ is given by

$$\psi(t') = \text{rect}\left(\frac{t'-\frac{\tau}{2}}{\tau}\right) \exp\left[j \frac{K}{2}\left(t'-\frac{\tau}{2}\right)^2\right], \tag{44}$$

where τ is the pulsewidth, and K is the linear FM rate in rad/s^2. For $\psi(t')$ given by (44),

$$g(\gamma) = (\tau-|\gamma|) \text{ rect}\left(\frac{\gamma}{2\tau}\right) \text{ sinc}\left[\frac{K}{2}(\tau-|\gamma|)\gamma\right], \tag{45}$$

where sinc $x = \sin x/x$.

The shape of $g(\gamma)$ is shown in Figure 6. The sinc$[K\gamma/2 (\tau-|\gamma|)]$ factor produces three peaks; the outer two of which are suppressed by the $(\tau-|\gamma|)$ factor. Provided the time-bandwidth product of the range (t') signal is high, i.e., provided $\gamma \ll \tau$ in the vicinity of $\gamma=0$, the major portion of the signal energy will be contained in the central peak. The equation describing the form of this peak can be closely approximated by

$$g(\gamma) \simeq \tau \text{ sinc}\left(\frac{K}{2} \tau\gamma\right). \tag{46}$$

The r_2 resolution is proportional to the mainlobe width (the width between the first null on each side of $\gamma=0$), which is given by
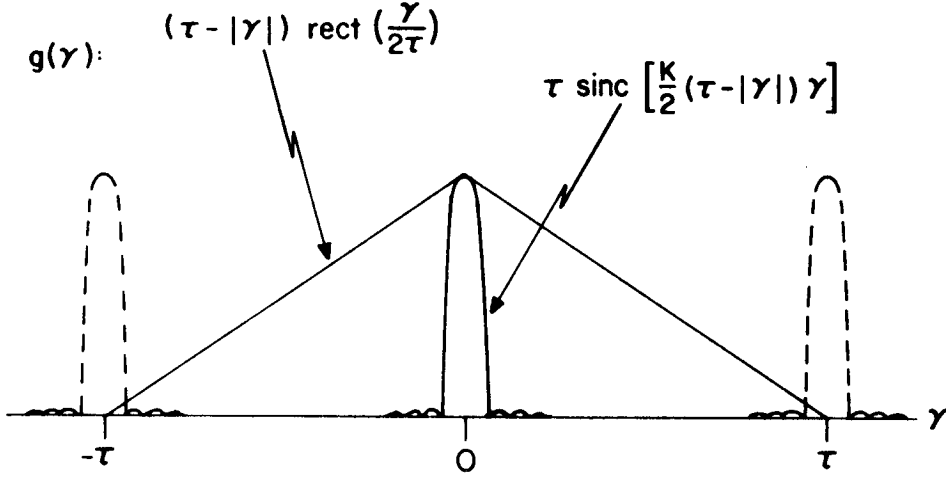
Figure 6. Form of Signal from a Single Point Target, After the Solution of the Inside Integral.

$$W_R = \frac{2\pi c}{K\tau} \tag{47}$$

It can be seen in Figure 6 that the position of the central peak produced by the solution of the inner integral is at $\gamma=0$. From (42) it is known that γ depends on $[a_1\xi-\tilde{a}_1(\xi-s)-a_2\xi^2-\tilde{a}_2(\xi-s)^2]$ which in turn, is a function of the azimuth (ξ) position. The ξ-dependence is a manifestation of the coupling or interdependence of the range (t') and along-track (s) signals.

4.2.2 Separation of Variables

In order to obtain an analytical solution to the outside integral in (41), γ in $g(\gamma)$ must be constrained such that the ξ-dependence is removed. If one lets

$$A_2 = a_2-\tilde{a}_2 \tag{48}$$

$$A_1 = a_1-\tilde{a}_1+2\tilde{a}_2 s \tag{49}$$

and

$$A_0 = a_0+\tilde{a}_1 s-\tilde{a}_2 s^2, \tag{50}$$

one can rewrite (42) as

$$\gamma = t' - \frac{2}{c}(A_2\xi^2+A_1\xi+A_0). \tag{51}$$

The ξ-dependence can be removed from (46) by choosing A_2 and A_1 in such a way that the position of the main peak does not deviate from $\gamma=0$, by more than a small fraction of its width; i.e., a small fraction of $2\pi c/K\tau$. This deviation is described by the following equation

$$\delta_r = \left| A_2 \xi^2 + A_1 \xi \right| \ll 2 \frac{\pi c}{K \tau}. \tag{52}$$

With the restriction given by (52), the substitution

$$\gamma = t' - \frac{2}{c}(A_0 \pm \delta_r) \tag{53}$$

can be made for γ in $g(\gamma)$, and an approximate analytical solution for (41) obtained.

4.2.3 Solution of the Outside Integral

The remaining step in the solution of (41) is the integration over ξ. With γ given by (53), (41) can be written as

$$f_o(t',s) = \frac{W_o \Gamma}{2} g\left[t' - \frac{2}{c}(A_0 \pm \delta_r)\right] \int_{\xi=-\infty}^{\xi=+\infty} rect\left(\frac{-s+\xi}{\tilde{L}_S}\right)$$

$$rect\left(\frac{\xi}{L_S}\right) \exp[-j2k(A_0 + A_1\xi + A_2\xi^2)]d\xi \quad . \tag{54}$$

The solution to (54) has two major cases, $A_2=0$ and $A_2 \neq 0$, and two sub-cases of each of the major ones, $\tilde{L}_S \geq L_S$ and $\tilde{L}_S < L_S$.

The variable A_2 has a special significance in that it determines the magnitude of the quadratic phase error, i.e.,

$$\Phi_e = 2kA_2\xi^2. \tag{55}$$

As shown in [15] the magnitude of the quadratic phase error determines whether or not an image can be considered focussed. In [15] the in-focus condition is defined by

$$|\Phi_e| \leq \frac{\pi}{8} \text{ rad} \quad . \tag{56}$$

In this section the solution for $A_2=0$ will be obtained, and then by reference to [15] it will be shown that for $A_2 \neq 0$ the solution gradually degrades as $|A_2|$ increases. With this link established, it will be assumed that the solution for $A_2=0$ can be used as long as the image is in focus.

For $\tilde{L}_S > L_S$, the impulse response of the matched filter is longer than the signal from which the synthetic-aperture is formed. It will be shown later that in certain situations $\tilde{L}_S$ must be greater than L_S in order to obtain the full along-track resolution.

For $\tilde{L}_S < L_S$, the impulse response of the matched filter is shorter than the signal from which the synthetic-aperture is formed. Sometimes $\tilde{L}_S$ is chosen to be smaller than L_S because the antenna along-track illumination is broader, and thus L_S is longer, than required to obtain the desired resolution.

4.2.3.1 Solution for Zero Quadratic Phase Error

1. $\tilde{L}_S \geq L_S$

For this sub-case the solution to (54) is given by

$$f_o(t',S) = \frac{W_o \Gamma}{2} g\left[t' - \frac{2}{c}(A_0 \pm \delta_r)\right] \exp(-j2kA_0)$$

$$\left\{ \text{rect}\left(\frac{s + \frac{\tilde{L}_S}{2}}{L_S}\right)\left(s + \frac{\tilde{L}_S + L_S}{2}\right) \exp\left\{jkA_1\left[-s - \left(\frac{\tilde{L}_S - L_S}{2}\right)\right]\right\} \right.$$

$$\text{sinc}\left[kA_1\left(s + \frac{\tilde{L}_S + L_S}{2}\right)\right] + \text{rect}\left[\frac{s}{(\tilde{L}_S - L_S)}\right]$$

$$L_S \text{ sinc}(kA_1 L_S) + \text{rect}\left[\frac{\left(s - \frac{\tilde{L}_S}{2}\right)}{L_S}\right]$$

$$\left(-s + \frac{\tilde{L}_S + L_S}{2}\right) \exp\left[jkA_1\left(-s + \frac{\tilde{L}_S - L_S}{2}\right)\right]$$

$$\left. \text{sinc}\left[kA_1\left(-s + \frac{\tilde{L}_S + L_S}{2}\right)\right] \right\}. \tag{57}$$

Figure 7 shows the form of (57). It can be seen that it is highly desirable to ensure that the position of the main peak of the azimuth response S_p, where

$$s_p = \frac{\tilde{a}_1 - a_1}{2\tilde{a}_2}, \tag{58}$$

is confined to the interval

$$\frac{(L_S - \tilde{L}_S)}{2} \leq s_p \leq \frac{(\tilde{L}_S - L_S)}{2}. \tag{59}$$

In this interval neither attenuation nor broadening of the main peak occurs, and the main peak width (i.e., between the nulls), is given by

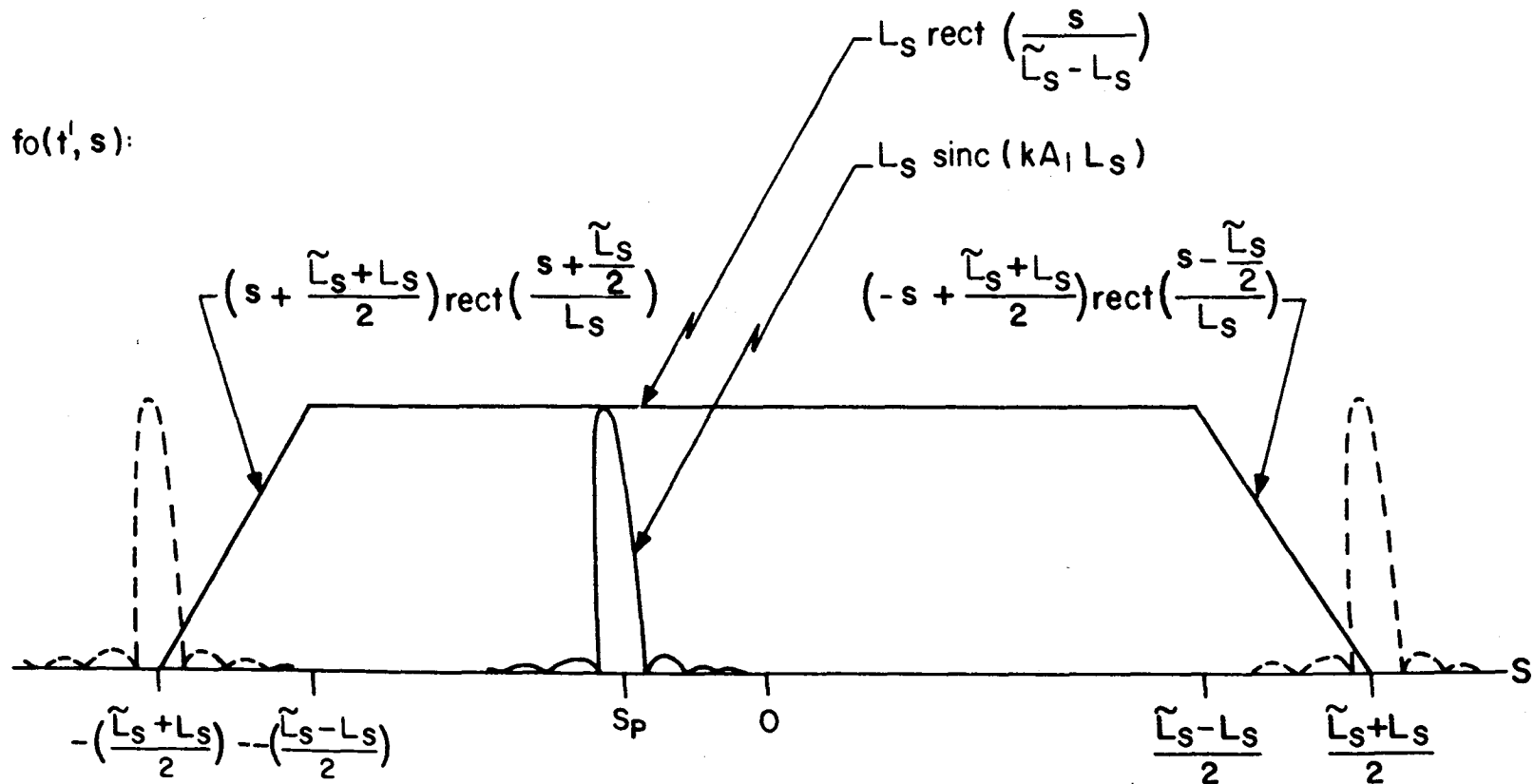$$W_{az} = \frac{\pi}{L_S k \tilde{a}_2}. \tag{60}$$

$fo(t', s):$

$L_S \, rect \left(\dfrac{s}{\tilde{L}_S - L_S} \right)$

$L_S \, sinc \, (kA_I \, L_S)$

$\left(s + \dfrac{\tilde{L}_S + L_S}{2} \right) rect \left(\dfrac{s + \dfrac{\tilde{L}_S}{2}}{L_S} \right)$

$\left(-s + \dfrac{\tilde{L}_S + L_S}{2} \right) rect \left(\dfrac{s - \dfrac{\tilde{L}_S}{2}}{L_S} \right)$

$-\left(\dfrac{\tilde{L}_S + L_S}{2} \right)$ $-\left(\dfrac{\tilde{L}_S - L_S}{2} \right)$ S_P O $\dfrac{\tilde{L}_S - L_S}{2}$ $\dfrac{\tilde{L}_S + L_S}{2}$ S

Figure 7. Form of Signal From a Single Point Target, After the Solution of the Outside Integral.

For (59) to hold, $\tilde{L}_S$ must be chosen such that

$$\tilde{L}_S \geq L_S + s_p.$$

(61)

2. $\tilde{L}_S < L_S$

For this sub-case the solution to (54) is given by

$$f_o(t',s) = \frac{W_o \Gamma}{2} g\left[t' - \frac{2}{c}(A_0 \pm \delta_r)\right]$$

$$\exp(-j2kA_0) \left\{ \text{rect}\left(\frac{s + \frac{L_S}{2}}{\tilde{L}_S}\right)\right.$$

$$\left(s + \frac{\tilde{L}_S + L_S}{2}\right) \exp\left\{jkA_1\left[-s - \left(\frac{\tilde{L}_S - L_S}{2}\right)\right]\right\}$$

$$\text{sinc}\left[kA_1\left(s + \frac{\tilde{L}_S + L_S}{2}\right)\right]$$

$$+ \text{rect}\left(\frac{s}{L_S - \tilde{L}_S}\right) L_S \exp(-2jkA_1 s)$$

$$\text{sinc}(kA_1\tilde{L}_S) + \text{rect}\left(\frac{s - \frac{L_S}{2}}{\tilde{L}_S}\right)$$

$$\exp\left[jkA_1\left(-s + \frac{\tilde{L}_S - L_S}{2}\right)\right]$$

$$\left. \text{sinc}\left[kA_1\left(-s + \frac{\tilde{L}_S + L_S}{2}\right)\right]\right\} .$$

(62)

When $\tilde{L}_S$ is chosen such that

$$L_S \geq \tilde{L}_S + s_p ,$$

(63)

the main peak width, between the nulls, is

$$W_{az} = \frac{\pi}{\tilde{L}_S k\tilde{a}_2} .$$

(64)

4.2.3.2 Solution for Non-Zero Quadratic Phase Error

The purpose of this section is to obtain the solution for (54), when $A_2 \neq 0$. By reference to [15] it is shown that as A_2 approaches zero, the solution to (54) gradually assumes the form of (57) or (62).

When $A_2 \neq 0$, the solution to (54) is found by solving the following integral

$$f_o(t',s) = \frac{W_o \Gamma}{2} g(\gamma) \exp\left[-j2k\left(A_o - \frac{A_1^2}{4A_2}\right)\right] \int_{\xi=-\infty}^{\xi=\infty} \text{rect}\left(\frac{-s+\xi}{\tilde{L}_S}\right) \text{rect}\left(\frac{\xi}{L_S}\right)$$

$$\exp\left[-j2kA_2\left(\xi + \frac{A_1^2}{2A_2}\right)^2\right] d\xi. \tag{65}$$

The solution to (65) has two sub-cases, $\tilde{L}_S > L_S$ and $\tilde{L}_S < L_S$. A link with (57) and (62) will be established by examining the solution for $\tilde{L}_S > L_S$. The solution for $\tilde{L}_S < L_S$ is found in a similar manner. When $\tilde{L}_S \geq L_S$, the solution to (65) is

$$f_o(t',s) = \frac{W_o \Gamma}{2} g(\gamma) \exp\left[-j2k\left(A_0 - \frac{A_1^2}{2A_2}\right)\right]$$

$$\frac{1}{2}\left(\frac{\pi}{kA_2}\right)^{\frac{1}{2}} \left\{ \text{rect}\left(\frac{s + \frac{\tilde{L}_S}{2}}{L_S}\right) \left\{[C(\xi_2') - C(\xi_1')] + j[S(\xi_2') - S(\xi_1')]\right\}\right.$$

$$+ \text{rect}\left(\frac{s}{\tilde{L}_S - L_S}\right) \left\{[C(\xi_4') - C(\xi_3') + j[S(\xi_4') - S(\xi_3')]]\right\}$$

$$\left. + \text{rect}\left(\frac{s - \frac{\tilde{L}_S}{2}}{L_S}\right) \left\{[C(\xi_6') - C(\xi_5')] + j[S(\xi_6') - S(\xi_5')]\right\}\right\}, \tag{66}$$

where

$$C(\xi') = \int_0^{\xi'} \cos\frac{\pi}{2} t^2 \, dt, \tag{67}$$

$$S(\xi') = \int_0^{\xi'} \sin\frac{\pi}{2} t^2 \, dt, \tag{68}$$

are Fresnel integrals, and

$$\xi_1' = \xi_3' = 2\left(\frac{kA_2}{\pi}\right)^{\frac{1}{2}} \left(-\frac{L_S}{2} + \frac{A_1}{2A_2}\right) \quad , \tag{69}$$

$$\xi_2' = 2\left(\frac{kA_2}{\pi}\right)^{\frac{1}{2}} \left(s + \frac{\tilde{L}_S}{2} + \frac{A_1}{2A_2}\right) \quad , \tag{70}$$

$$\xi_4' = \xi_6' = 2\left(\frac{kA_2}{\pi}\right)^{\frac{1}{2}} \left(\frac{L_S}{2} + \frac{A_1}{2A_2}\right) \quad , \tag{71}$$

and

$$\xi_5' = 2\left(\frac{kA_2}{\pi}\right)^{\frac{1}{2}} \left(s - \frac{\tilde{L}_S}{2} + \frac{A_1}{2A_2}\right) \quad . \tag{72}$$

The second term in (66) represents the solution when the main peak is located in the region $(L_S-\tilde{L}_S)/2$ to $(\tilde{L}_S-L_S)/2$. In this region (66) becomes

$$f_o'(t',s) = \frac{W_o \Gamma}{2} g(\gamma) \exp\left[-j2k\left(A_0 - \frac{A_1^2}{4A_2}\right)\right]$$

$$\frac{1}{2}\left(\frac{\pi}{kA_2}\right)^{\frac{1}{2}} \text{rect}\left(\frac{s}{\tilde{L}_S-L_S}\right) \left\{[C(P) - C(Q)] + j[S(P) - S(Q)]\right\} , \tag{73}$$

where, using the notation of [15],

$$P = \frac{1}{\sqrt{\pi}}\left(\frac{\Delta t}{2n} + n\right) = \xi_4' \quad , \tag{74}$$

$$Q = \frac{1}{\sqrt{\pi}}\left(\frac{\Delta t}{2n} - n\right) = \xi_3' \quad , \tag{75}$$

and

$$\frac{\Delta t}{2} = A_1 k L_S \tag{76}$$

and

$$n = L_S \sqrt{kA_2} = \sqrt{2\Phi_{e_{max}}} \quad . \tag{77}$$

The substitution in terms of Δt, and n allows comparison of (73) with the results in [15]. In [15], it is shown that as $\Phi_{e_{max}}$ decreases from $\pi/8$ rad to 0 rad only a slight change in the shape of the main compression peak occurs. Similarly, the solutions (57) and (62) degrade only slightly as

$|A_2| \to \pi/8$ rad. Thus, for $\Phi_{e_{max}} \leq \pi/8$ rad (57) and (62) can be used as the general solution to (54).

4.3 PROCESSING SWATH IN RANGE

The allowable processing swath in range Δr_1 over which a single matched filter can be used, it determined by the maximum range mismatch which satisfies both the restriction on Φ_e, (56), and the equation for δ_r, (52).

4.3.1 $\Phi_{e_{max}}$ Restriction

As can be seen from (55), the maximum quadratic phase error occurs at ξ_{max} which from (54) is

$$\xi_{max} = \frac{L_S}{2} \quad . \tag{78}$$

The maximum value of

$$\Delta r_1 = 2|r_1 - \tilde{r}_1| \quad , \tag{79}$$

is found by solution of the following equation:

$$\left| 2kA_2 \left(\frac{L_S}{2} \right)^2 \right| \leq \frac{\pi}{8} \quad , \tag{80}$$

where Φ_e has been replaced by (55), and ξ by (78). After the substitution of (48) for A_2, and of (32) for k, (80) can be written as

$$\frac{8L_S^2}{\lambda} |a_2 - \tilde{a}_2| \leq 1 \quad , \tag{81}$$

After replacement of a_2 and $\tilde{a}_2$ in (81), the equation can be rewritten as

$$\frac{8L_S^2}{\lambda} \left| \frac{1}{2r_1} \left[\frac{1 + C_a^2}{2} - \frac{r_1^2}{2r_e^2} - \frac{r_e^2}{r_1^2} C_a^2 \frac{\sin^2\theta_r}{\tan^2\alpha} \right] \right.$$

$$\left. - \frac{1}{2\tilde{r}_1} \left[\frac{1 + C_a^2}{2} - \frac{\tilde{r}_1^2}{2r_e^2} - \frac{r_e^2}{\tilde{r}_1^2} C_a^2 \frac{\sin^2\tilde{\theta}_r}{\tan^2\tilde{\alpha}} \right] \right| \leq 1. \tag{82}$$

If it is assumed that $(r_1^2/r_e^2) \ll 1$, and $\alpha = \tilde{\alpha}$, then (82) can be simplified to

$$\frac{2L_S^2}{\lambda} \left| \left(-\frac{1 + C_a^2}{2} + C_a \cos^2\alpha \right) \frac{\pm\Delta r_1}{\left(\tilde{r}_1 \pm \frac{\Delta r_1}{2} \right) \tilde{r}_1} \right.$$

$$\left. -C_a h_s^2 \cos^2\alpha \left[\frac{\tilde{r}_1^3 - \left(\tilde{r}_1 \pm \frac{\Delta r_1}{2} \right)^3}{\tilde{r}_1^3 \left(r_1 \pm \frac{\Delta r_1}{2} \right)^3} \right] \right| \leq 1. \tag{83}$$

If the further assumption $\Delta r_1/2 \ll \tilde{r}_1$ can be made, then (83) can be rearranged to give Δr_1 explicitly, i.e.,

$$\Delta r_1 \leq \frac{\lambda \tilde{r}_1}{2L_S^2} \frac{1}{\left| \frac{1 + C_a^2}{2} - C_a \cos^2\alpha + \frac{3C_a h_s^2 \cos^2\alpha}{\tilde{r}_1^2} \right|} . \tag{84}$$

Otherwise, the solution for Δr_1 must be found from (82) or (83).

For the case $\tilde{L}_S \geq L_S$, the value of L_S is found from (65) to be

$$L_S = \frac{\lambda}{2W_{az} \tilde{a}_2} . \tag{85}$$

If the same approximations used in (83) and (84) are used in the substitution for $\tilde{a}_2$ in (85), (84) can be rewritten as

$$\Delta r_1 \leq \frac{W_{az}^2}{2\lambda} \left| \frac{\left[\frac{1+C_a^2}{2} - C_a \cos^2\alpha + \frac{C_a h_s^2}{\tilde{r}_1^2} \cos^2\alpha \right]^2}{\frac{1+C_a^2}{2} - C_a \cos^2\alpha + \frac{3C_a h_s^2}{\tilde{r}_1^2} \cos^2\alpha} \right| \tag{86}$$

From (86) it can be seen that for moderate squint, i.e., $\alpha \simeq 90°$, the range swath is determined by

$$\Delta r_1 \leq \frac{W_{az}^2}{2\lambda} \left(\frac{1 + C_a^2}{2} \right) . \tag{87}$$

A large squint angle, i.e., small α, coupled with a steep depression angle, i.e., $h_s/r_1 = 1$, causes Δr_1 to be decreased from the value given in (87). This combination of small α and $h_s/r_1 \simeq 1$ represents the most severe operating geometry with respect to the range swath Δr_1, that can be processed with a single matched filter.

4.3.2 δ_r Restriction

In this section it is shown that a suitable δ_r can be found to satisfy (52). Bounds have already been placed on ξ (78), and A_2 (80). Thus the only step remaining is the derivation of a bound on A_1. The validity of the solution to (40) is restricted to a neighborhood of radius $2 W_{az}$ about the main compresion peak. With this restriction, $|A_1|$ is limited to the interval

$$|A_1| \le |a_1 - \tilde{a}_1 + 2\tilde{a}_2(s_p \pm 2 W_{az})|. \tag{88}$$

After substitution for s_p (59), and W_{az} ((60) or (64)), (88) can be written

$$|A_1| \le |\lambda|. \tag{89}$$

If the restriction (89) is coupled with those on A_2 (80) and ξ (78), then (52) can be rewritten as

$$\delta_r = \left|\frac{\lambda}{32} \pm \lambda\right| << W_r, \quad \tilde{L}_S \ge L_S, \tag{90}$$

or

$$\delta_r = \left|\frac{\lambda}{32} \pm \lambda \frac{\tilde{L}_S}{L_S}\right| << W_r, \quad \tilde{L}_S < L_S. \tag{91}$$

Equations (90) and (91) give the maximum value of δ_r. The width W_r is always much greater than λ because of fundamental physical constraints. Therefore the solutions given by (57) and (62) are only constrained by the quadratic phase error restriction (56). Henceforth, the quadratic phase error restriction will be considered as the only restriction.

The restriction on δ_r ensures that no additional energy is spilled into the two-dimensional sidelobe structure by the range-azimuth coupling. The solutions obtained subject to this restriction do not provide any insight as to the detailed form of this sidelobe structure. The sidelobes can only be fully described by a numerical solution of (41).

4.4 PROCESSING INTERVAL IN AZIMUTH

In the along-track or azimuth dimension, there are also restrictions on the processing swath. As the vehicle carrying the radar moves along its track it will, in general, traverse lines of constant latitude. The latitude change introduces a change in θ_{ye}, and therefore α. If α changes appreciably in value from $\tilde{\alpha}$, the reference function (40) will no longer match the properties of the signal received by the antenna. The length of the reference function $\tilde{L}_S$ must be chosen according to (63) so that it is long enough to properly match the data that is received.

4.5 POSITIONAL ERRORS IN COMPRESSED SIGNAL

In this section it is shown that the two-dimensional convolution selects portions of the signal f_D with slope $\tilde{a}_1$. These selected portions

24

are shown to be offset in r_1 and s from the centre of the two-dimensional signal returned from the target.

The selection process can be understood by examining Figure 8. In Figure 8 are shown three sets of lines: the dotted is a line of constant $\tilde{a}_1$; the solid are lines of constant S; and the dashed are lines of constant r_o. The slopes of the dashed lines are given by

$$\frac{dr_2}{ds} = a_1 + 2a_2 s \quad . \tag{92}$$

For the particular line through D, (92) can be written as

$$\frac{d\tilde{r}_2}{ds} = \tilde{a}_1. \tag{93}$$

Equation (93) is the slope of the phase fronts of the two-dimensional reference function $h_3(t',o)$. The two-dimensional convolution will cause a section of $f_D(t',s)$ to be selected that has a slope $\tilde{a}_1$. It is known from (64) that the compression peak, for a target located along the line $s=0$ (e.g., E in Figure 8), will be located at s_p (e.g., F in Figure 8). For $a_2 \simeq \tilde{a}_2$ the slope at F is

$$\frac{dr_2}{ds} = \tilde{a}_1 = \left. \frac{d\tilde{r}_2}{ds} \right|_{s=0} \quad , \tag{94}$$

where $d\tilde{r}_2/ds \big|_{s=0}$ is the slope at D, the point to which the reference function is matched. Since the locations of the points E and F are general, it can be stated that the convolution does indeed select portions of $f_D(t',s)$ with the same slope as $h_3(t',s)$ at D.
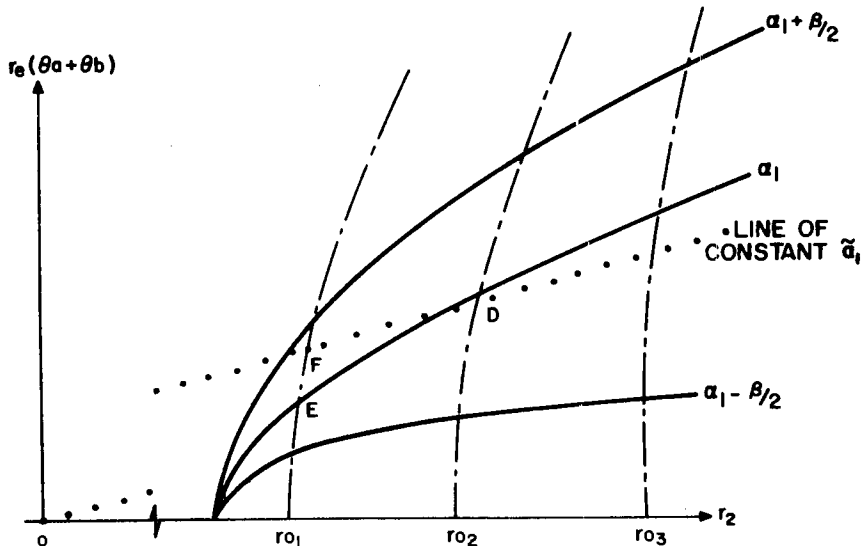

Figure 8. Form of the Isodops

In Figure 8 it is shown that the output signal is also shifted in range by the displacement from E to F. The output position, as seen in (53), is shifted from a_0 to $A_0 \pm \delta_r$, where

$$A_0 = a_0 + \Delta r(s_p), \tag{95}$$

and

$$\Delta r(s_p) = \tilde{a}_1 s_p - \tilde{a}_2 s_p^2. \tag{96}$$

Both the r_1-shift $\Delta r(s_p)$, and the s-shift s_p, are range dependent. They must be removed in order to form a geometrically correct image.

5. IMAGE FORMATION

In order to form a geometrically correct image, the azimuth offsets s_p (59), and the range offsets $\Delta r(s_p)$ (96), must be removed. After removal of these offsets, a line of points, e.g., AS_1' in Figure 9, will lie along a line of constant s in the (r_1,s) coordinate system, i.e., will be plotted perpendicular to s. When viewed from the (d_o,s_o) coordinate system, where (d_o,s_o) forms an orthongonal map grid on the surface of the planet, the axes r_1 and s are neither coplanar nor orthogonal. Therefore when an orthogonal map is required, images produced in the (r_1,s) coordinate system must undergo a coordinate transformation. This transformation involves two operations:

1. conversion from slant range r_1 to ground range d_1, and

2. conversion from processor coordinates (d_1,s) to map coordinates (d_o,s_o).

Ground range is obtained from slant range by using the equation

$$d_1 = r_e \cos^{-1}\left[\frac{\left(\dfrac{r_1}{r_e}\right)^2 - C_a^2 - 1}{-2C_a}\right] \tag{97}$$

The conversion from (d_1,s) to (d_o,s_o) is made by writing the constant s line (AS_1 in Figure 9) at an angle with respect to the sub-satellite track $(s_o s_1)$. The data must be laid down on the map along the lines described by the intersection of the antenna centre-beam plane and the surface of the earth, when the satellite is at orbital position $\theta_a(r_e+h_s)$. The equations which describe the transformation are

$$d_o = r_e \sin^{-1}\left[\sin\left(\frac{d_1}{r_e}\right)\sin\alpha\right], \tag{98}$$

and

$$s_o = s - r_e \sin^{-1}\left(\frac{\tan\theta_r}{\tan\alpha}\right). \tag{99}$$

Figure 10 shows the relationship of d_1, d_0, s and s_0 for a target located at A.
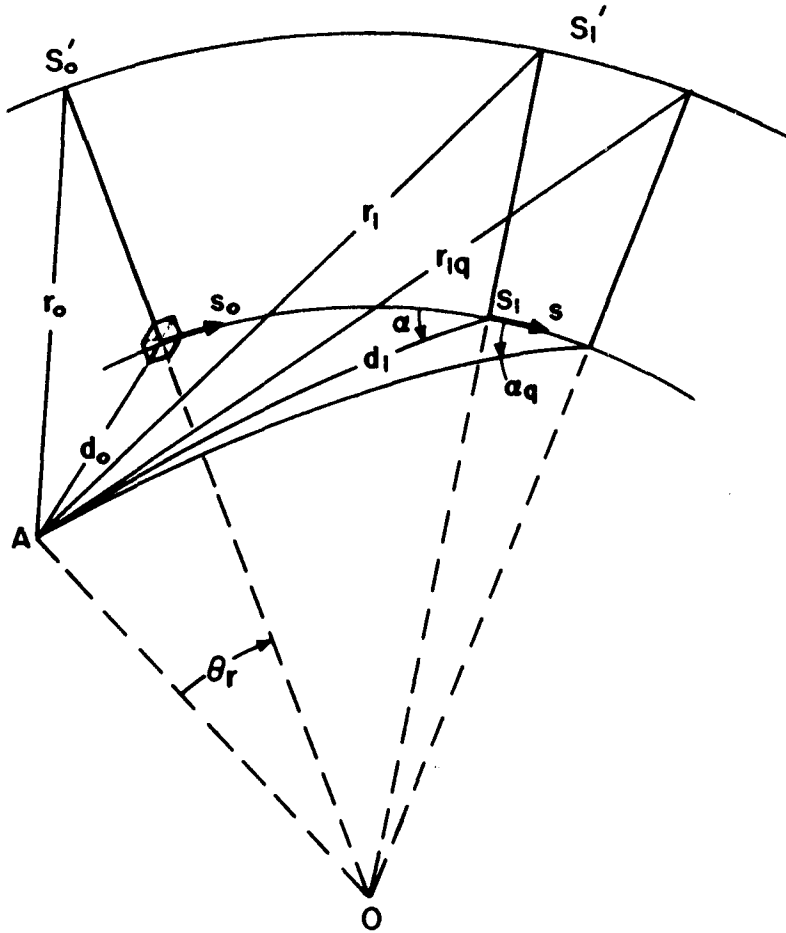

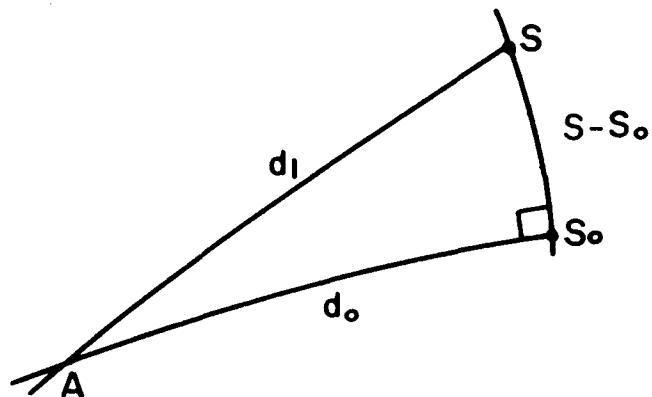*Figure 9. Radar Geometry for Multilook Processing*

Figure 10. Transformation From Squinted to Sidelooking Ground Coordinates

6. MULTI-LOOK SIGNAL PROCESSING

This section describes multi-look signal processing, a technique that is employed in SAR to reduce target scintillation.

In Section 3.3 it was shown, (see eqn. 64)) that the azimuthal resolution is proportional to the length of the signal function that is used to form the synthetic-aperture. Frequently, the antenna beamwidth β is sufficiently broad that the resulting signal function is longer than that required to produce the desired azimuth resolution. Rather than truncating the signal and thereby wasting the energy associated with this additional signal, it is common practice to segment it into several pieces, each of appropriate length for the resolution desired. Each of these segments is matched-filtered to produce an image.

The images are geometrically corrected and converted to map coordinates. After registering the images with respect to one another, they are noncoherently summed together to form a composite image. The terms multi-looking, angle diversity, and mixed integration are the jargon commonly used to describe the noncoherent averaging operation.

The segmenting operation described above results in using portions of the azimuth signal that are acquired at different α-angles, (see Figure 9). Each of these images are referred to as "looks"; the qth look being at angle α_q. Obviously the α_q's must be selected such that the corresponding signal segments are contained within the antenna horizontal beamwidth.

In order to register the looks, it is necessary to specify the matched filters for each of the looks so that each filter corresponds to the same point A. To specify the qth filter, α_q is first selected, subject to the constraint mentioned above, and a_{0q}, a_{1q}, and a_{2q} are calculated using r_{1q} and α_q. The parameter r_{1q} is the slant range to A when A is at an angle-to-track α_q. In terms of the fundamental parameters α and r_1, r_{1q} is given by

$$\frac{r_{1q}^2}{r_e^2} = \left[C_a^2 + 1 - 2C_a \left\{ 1 - \frac{\sin^2\alpha}{\sin^2\alpha_q} \left(1 - \left[\frac{C_a^2 + 1 - \frac{r_1^2}{r_e^2}}{2C_a} \right]^2 \right)^{\frac{1}{2}} \right\} \right]^{\frac{1}{2}} \tag{100}$$

The qth filter is then specified by

$$a_{0q} = r_{1q} \ , \tag{101}$$

$$a_{1q} = \left(\frac{r_e}{r_{1q}} \right) C_a \frac{\sin\theta_r}{\tan\alpha_q} \ , \tag{102}$$

and

$$a_{2q} = \left[\frac{1}{2r_{1q}} \frac{1 + C_a^2}{2} - \frac{1}{2} \left(\frac{r_{1q}}{r_e} \right)^2 - a_{1q}^2 \right] \quad , \tag{103}$$

where

$$\sin\theta_r = \left[1 - \left(\frac{1 + C_a^2 - \dfrac{r_1^2}{r_e^2}}{2C_a} \right)^2 \right]^{\frac{1}{2}} \sin\alpha. \tag{104}$$

The matched filtering and image formation operations for the multi-look case, are identical to those required for the single look case, except that in all the equations the parameters a_{0q}, a_{1q}, a_{2q}, α_q and r_{1q} are substituted for a_0, a_1, a_2, α, and r_1.

7. EXAMPLE

A software digital processor based on the theory described in this report has been programmed and used to produce imagery from data acquired with airborne and satellite-borne SARs. Examples of processed imagery are shown in Figures 12 and 13. The images were produced using data from the SEASAT-A satellite. The image in Figure 12 is a four-look 25m ground range x 25m azimuth resolution image of Trois Rivieres, Quebec. The image in Figure 13 is a single-look 25m ground range x 7m azimuth resolution image of Halifax, Nova Scotia. The processing parameters for these two scenes are given in Table 1. For the SEASAT-A satellite the antenna beam is only slightly squinted (3-4°); however, the relatively low frequency (1.276 GHz) of the transmitted signal, and the large distance between the satellite and the planet's surface, mean that processing the data to 7 and 25m resolutions involves the same degree of complexity as more highly squinted airborne systems.
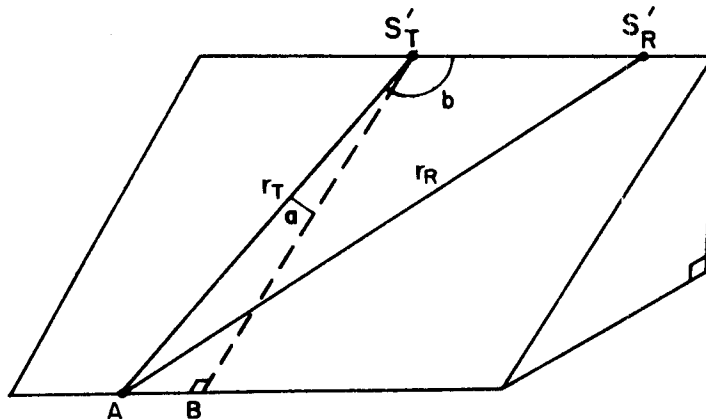

Figure 11. Definition of Slant Ranges at Transmit and Receive Times

TROIS RIVIERES, QUEBEC
ORBIT 1181   SEP 17, 1978
25M RA X 25M AZ RESOLUTION - 4 LOOKS

AZIMUTH

GROUND RANGE

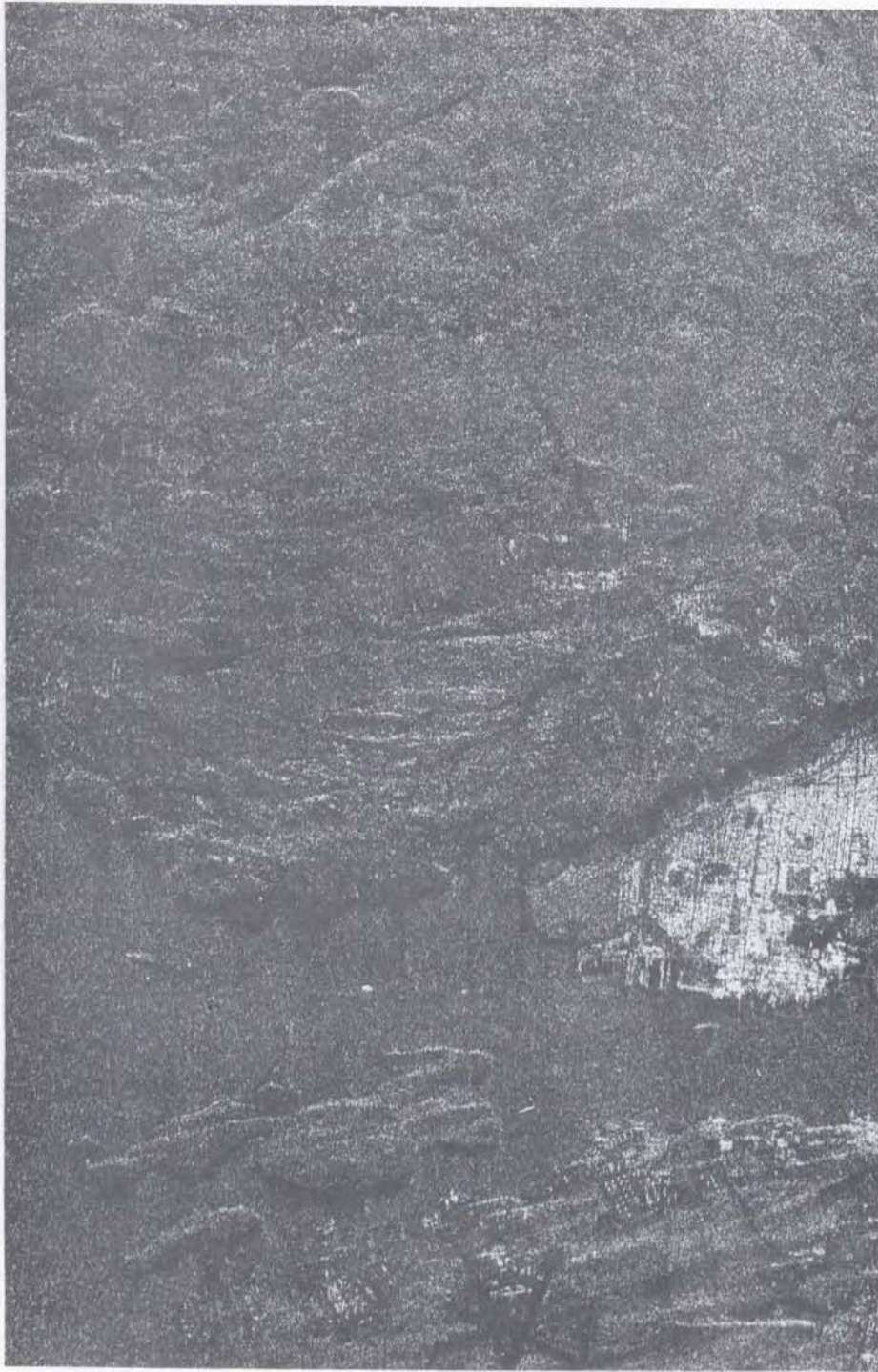Figure 12. SEASAT-A SAR Image of Trois Rivieres, Quebec

Figure 13. SEASAT-A SAR Image of Halifax, Nova Scotia

TABLE 1

Processing Parameters for Imagery Examples

Parameter	Halifax (7m az) 1-Look	Trois Rivieres (25m az) 4-Look
h_s	796.529 km	796.853 km
r_e	6368.110 km	6367.623 km
V_{eq}	6775.349 $\frac{m}{s}$	6774.502 $\frac{m}{s}$
α	86.629°	87.860°
r_1	851.062 km	866.781 km
$\frac{\omega_c}{2\pi}$	1.276 GHZ	1.276 GHz
$\frac{1}{T}$	1646.7603 Hz	$\frac{1646.7603}{4}$
L_s	13.52 km	4.13 km
$\frac{K}{2\pi}$	-0.56275 $\frac{MHz}{\mu sec}$	-0.56275 $\frac{MHz}{\mu sec}$
τ	33.9 μsec	33.9 μsec
W_R	15.7m	15.7m
W_{az}	13.2m	43.9m
Δr_1 (approx.)	0.25 km	4.0 km
$\alpha_q - \alpha_{q-1}$	---	0.516°

8. SUMMARY

A general theory of two-dimensional SAR processing has been presented. The forms of the range and azimuth radar signals returned from a general point target have been derived, and it has been shown that these signals are not in general independent, i.e., they are coupled. An approximate closed form solution describing the image produced by performing a two-dimensional convolution of the SAR signal, returned from a point target, with the two-dimensional impulse response of the matched filter has also been given. By means of this solution it has been shown that a single two-dimensional reference function can be used to produce high quality images from radar signals obtained over a swath in range. However, these images must be geometrically corrected to remove positional errors introduced by the processing. Equations have been developed to describe both the positional

errors and the operations required to remove them. Finally, the modifications required to extend the theory to include the case of multi-look processing, or noncoherent averaging have been developed.

9. ACKNOWLEDGEMENT

10. REFERENCES

1.   Leith, E.N., *Quasi-Holographic Techniques in the Microwave Region*, Proc. IEEE, Vol. 59, No. 9, September 1971.

2.   Brown, W.M., *Synthetic-aperture Radar*, IEEE Trans. Aerosp. Electron, Syst., Vol. AES-3, pp. 217-229, March 1967.

3.   Brown, W.M. and L.J. Porcello, *An Introduction to Synthetic-aperture Radar*, IEEE Spectrum, Vol. 6, pp. 52-62, September 1969.

4.   Cutrona, L.J., *Synthetic-aperture Radar*, in Radar Handbook, M.I. Skolnik, Ed., New York: McGraw-Hill, 1970, Ch. 23, pp. 23.1-23.25.

5.   Harger, R.O., *Synthetic Aperture Radar Systems*, Theory and Design, New York: Academic Press, 1970.

6.   Kovaly, J.J., *Synthetic Aperture Radar*, Dedham, MA: Artech House, 1976.

7.   Brookner, E., *Radar Technology*, Dedham, MA: Artech House, 1977.

8.   Tomiyasu, K., *Tutorial Review of Synthetic-aperture Radar (SAR) With Applications to Imaging of the Ocean Surface*, Proc. IEEE, Vol. 66, pp. 563-583, May 1978.

9.   Leith, E.N., *Range-azimuth Coupling Aberrations on Pulse-scanned Imaging Systems*, J.O.S.A., Vol. 63, pp. 119-126, February 1973.

10.   Wu, C., *Electronic SAR Processors for Space Missions*, Paper No. V-3, in Proceedings of the Synthetic Aperture Radar Technology Conference, Alberquerque, NM., 8-10 March 1978.

11.   Wu, C., *A Digital Approach to Produce Imagery From SAR Data*, AIAA Paper No. 76-968, Proceedings of the AIAA System Design Driven by Sensors Conference, Pasadena, CA., October 1976.

12.   van de Lindt, W.J., *Digital Technique for Generating Synthetic-aperture Radar Images*, IBM J. Res. and Develop., Vol. 21, pp. 415-432, September 1977.

13. Bennett, J.R. and R. Orth, *An Approach to the Design of a Digital Ground Data Processor for Satellite-borne Synthetic-aperture Radar*, presented at Sixth Canadian Symposium on Remote Sensing, Victoria, B.C., 28-31 August 1978.

14. Kirk, J.C., *A Discussion of Digital Processing in Synthetic-aperture Radar*, IEEE Trans, AES, Vol. AES-11, pp. 326-337, May 1975.

15. Klauder, J.R., A.C. Price, S. Darlington, and W.J. Albersheim, *The Theory and Design of Chirp Radars*, Bell Sys. Tech. J., Vol. 39, pp. 745-808, July 1960.

A P P E N D I X   A

Derivation of V_{en} and V_{ep}

A brief derivation of (4) and (5) are given here. Refer to Figure 1. From rules of spherical trigonometry for right spherical triangles one has

$$\cos\phi_s = \frac{\sin(\pi-\theta_i)\cos\phi_o}{[1 - \sin^2(\pi-\theta_i)\sin^2\phi_o]^{\frac{1}{2}}} \quad , \quad \theta_i \neq \pi/2 \text{ rad.} \tag{A.1}$$

$$= 0, \quad \theta_i = \pi/2 \text{ rad.}$$

and

$$\sin(\pi-\theta_i) = \sin\phi_{lat}/\sin\phi_o. \tag{A.2}$$

The velocity components are

$$V_{en} = (\omega_e r_e \cos\phi_{lat})\cos\phi_s \tag{A.3}$$

and

$$V_{ep} = (\omega_e r_e \cos\phi_{lat})\sin\phi_s, \tag{A.4}$$

where ω_e is the planet rotational frequency. After some manipulation and the use of $\sin\phi_s = \sqrt{1-\cos^2\phi_s}$, (4) and (5) are obtained.

A P P E N D I X   B

Range as a Function of Orbital-Position in the Presence of an Orbital Vertical Velocity Component

To include a vertical velocity component, V_v, in (17) h_s is replaced by $h_s + V_v s/V_{eq}$. The second term is the radial displacement from the circular orbit undergone by the spacecraft in sweeping through the angle θ_b. The range r_2 then becomes

$$r_2 = \left\{ r_e + \left(r_e + h_s + \frac{V_v}{V_{eq}} s \right)^2 - 2r_e \left(r_e + h_s + \frac{V_v}{V_{eq}} s \right) \right.$$

$$\left. [\cos\theta\cos\theta_b - \sin\theta\cos\alpha\cos\theta_b] \right\}^{\frac{1}{2}} \qquad (B.1)$$

When the first three terms of the Maclaurin series are derived from the equation for r_2, as in Section 2, the a-coefficients are seen to be

$$a_0 = r_1 \qquad (B.2)$$

$$a_1 = \frac{r_e}{r_1} \left\{ C_a \frac{\sin\theta_r}{\tan\alpha} + \frac{V_v}{V_{eq}} C_a - \frac{V_v}{V_{eq}} \cos\theta \right\} \qquad (B.3)$$

$$a_2 = \frac{1}{2r_1} \left\{ \frac{1 + C_a^2}{2} - \frac{1}{2} \left(\frac{r_1}{r_e} \right)^2 - a_1 + \left(\frac{V_v}{V_{eq}} \right)^2 - 2 \left(\frac{V_v}{V_{eq}} \right) \frac{\sin\theta_r}{\tan\alpha} \right\} \qquad (B.4)$$

APPENDIX C

Derivation of Equation Describing the Transit Time

The distance travelled between transmission and reception of a pulse is (see Figure 11)

$$S'_T S'_R = \left(\frac{r_T + r_R}{c}\right) V_{eq}, \tag{C.1}$$

where r_T and r_R are the ranges to the target at the times of pulse transmission and reception, respectively. Then, following the treatment of [12], the range at the time of transmission if

$$r_T = \frac{\overline{AB}}{\sin a}, \tag{C.2}$$

where $\overline{AB}$ is the distance between A and B, and 'a' is the angle between BS'_T and AS'_T as shown in Figure 11. The angle 'b' between $S'_T S'_R$ and $S'_T A$ is related to 'a' as follows

$$\sin a = - \cos b. \tag{C.3}$$

Therefore, the range at the time of reception is found from the solution of

$$r_R^2 = r_T^2 + \left[\frac{V_{eq}}{c}(r_T + r_R)\right]^2 - 2r_T \frac{V_{eq}}{c}(r_T + r_R)\cos b \tag{C.4}$$

which can also be written as

$$r_R^2 = r_T^2 + \left[\frac{V_{eq}}{c}(r_T + r_R)\right]^2 + 2r_T \frac{V_{eq}}{c}(r_T + r_R)\frac{\overline{AB}}{r_T}. \tag{C.5}$$

If one factors $r_R^2 - r_T^2$ into $(r_R - r_T)(r_R + r_T)$, and divides both sides by $(r_R + r_T)$, the following equations are obtained

$$r_R = r_T \frac{\left[1 + \left(\frac{V_{eq}}{c}\right)^2\right]}{\left[1 - \left(\frac{V_{eq}}{c}\right)^2\right]} + 2\frac{V_{eq}}{c}\frac{\overline{AB}}{1 - \left(\frac{V_{eq}}{c}\right)^2}, \tag{C.6}$$

and

$$r_R + r_T = \frac{2r_T}{1 - \left(\dfrac{V_{eq}}{c}\right)^2} + 2\frac{V_{eq}}{c}\frac{\overline{AB}}{1 - \left(\dfrac{V_{eq}}{c}\right)^2} \ . \tag{C.7}$$

Thus

$$\Delta t = \frac{r_R + r_T}{c} = \frac{1}{C}\frac{2r_T}{1 - \left(\dfrac{V_{eq}}{c}\right)^2} + 2\frac{V_{eq}}{C}\frac{\overline{AB}}{1 - \left(\dfrac{V_{eq}}{c}\right)^2} \ . \tag{C.8}$$

Since (V_{eq}/c) is always much smaller than unity and usually $\overline{AB} \ll r_T$, the equation

$$\Delta t \simeq \frac{2r_T}{c} \tag{C.9}$$

is a very good approximation to (C.8).

VANT, MALCOLM R.

A theory of 'squinted'
aperture radar.

Date Due

MAY 4 1981		
JUN 10 1981		

FORM 109